The Conformation of Loop E of Eukaryotic 5S Ribosomal RNA†

Brian Wimberly,‡ Gabriele Varani,§ and Ignacio Tinoco, Jr.*

Department of Chemistry and Laboratory of Chemical Biodynamics, University of California, Berkeley, California 94720

Received August 28, 1992; Revised Manuscript Received October 20, 1992

ABSTRACT: The solution structure of a 27-nucleotide duplex, including the internal loop E from *Xenopus laevis* 5S ribosomal RNA, has been studied by two-dimensional NMR spectroscopy, followed by restrained molecular dynamics. The highly conserved internal loop closes to form a G·A base pair and a reverse-Hoogsteen A·U base pair. Extensive interstrand stacking between these uncommon base pairs provides a structural explanation for an interstrand ultraviolet-induced cross-link. A guanosine residue is bulged into the major groove and may form a base-triple with the adjacent reverse-Hoogsteen A·U pair. The structure of the less highly-conserved portion of the loop is less well-defined by the NMR data. A single-nucleotide deletion mutant has a very different, open conformation without mismatched base pairs [Varani, G., Wimberly, B., & Tinoco, I. Jr. (1989) *Biochemistry 28*, 7760–7772]. The implications of the structure for binding of the transcription factor TFIIIA and the cytotoxin α-sarcin are discussed.

Many of the diverse biological functions of RNA, including catalysis (Cech, 1990; Noller et al., 1992) and ligand binding (Ellington & Szostak, 1990; Puglisi et al., 1992), are thought to depend on unique three-dimensional conformations. While several hundred protein structures are known, only a few high-resolution RNA structures have been determined. Indeed, only a single tertiary structure, that of transfer RNA, is known at atomic resolution (Saenger, 1984), and the loop conformations of the RNA secondary structure elements (hairpin loops, internal loops, etc.) are only beginning to be determined (Chastain & Tinoco, 1991). The structures of internal loops are particularly poorly understood despite their functional importance as sites for protein binding (Stern et al., 1989; Gregory et al., 1988; Heaphy et al., 1991). Only one high-resolution structure has been reported for a symmetric internal loop that closes to form U·G and U·C mismatches (Holbrook et al., 1991).

One of the most-studied internal loops is loop E from the eukaryotic 5S ribosomal RNA (5S rRNA). This asymmetric loop comprises part of the binding site for at least two proteins, the transcription factor TFIIIA (Romaniuk, 1989) and the ribosomal protein L5 (Allison et al., 1991). The loop sequence is unusually highly conserved. A 5′-GUA-3′/3′-AG-5′ sequence motif is common to all eukaryotic 5S rRNAs and is also conserved in other internal loops (Figure 1); this suggests that there is a family of loop E-like structures. Irradiation with ultraviolet light induces the same interstrand cross-link in the human 5S rRNA loop E and in a very similar internal loop from the potato spindle tuber viroid (Figure 1B,C; Branch et al., 1985).

The conformation of loop E from the *Xenopus laevis* oocyte 5S rRNA has been investigated by measuring the reactivity of the bases and phosphates to various chemical and enzymatic reagents (Andersen et al., 1984; Romaniuk et al., 1988;

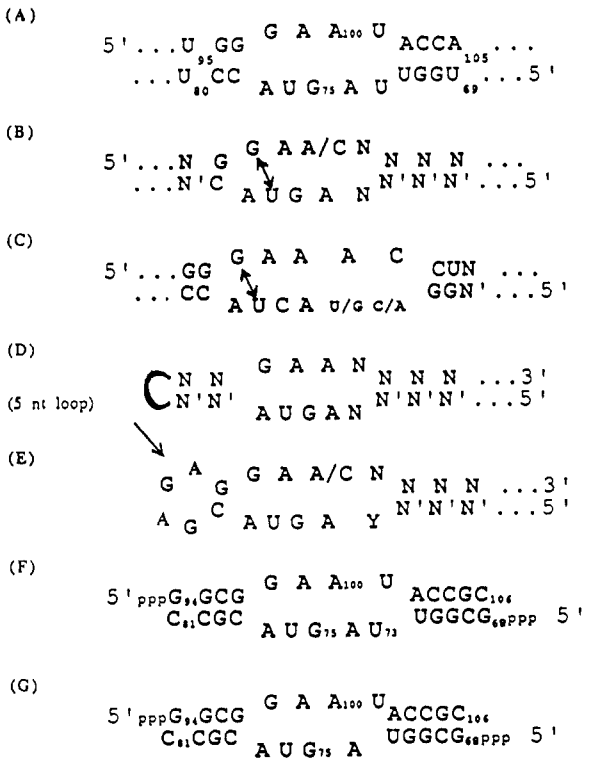

FIGURE 1: Sequence conservation in loop E-like internal loops. N is any nucleotide; Y is either C or U. N·N′ is a Watson–Crick or G·U base pair. Double-headed arrows connect bases covalently joined by an ultraviolet-induced cross-link in the human 5S rRNA loop E and in a viroid internal loop (Branch et al., 1985). Consensus sequences were obtained by comparison of the sequences reported by Wolters and Erdmann (1988), by Gutell and Fox (1988), and by Keese and Symons (1985). (A) Loop E from the *Xenopus laevis* oocyte 5S rRNA. (B) Loop E consensus from eukaryotic 5S rRNAs. (C) Consensus of loop sequences from the conserved central region of viroid RNAs. (D) Consensus of nonmitochondrial loop sequences from the 5′-end region (ca. residue 250 in the *Escherichia coli* numbering) of 23S-like rRNAs. (E) Consensus of nonmitochondrial loop sequences from the 3′-end region (ca. residue 2660 in the *E. coli* numbering) of 23S-like rRNAs. The arrow indicates the position of cleavage by the cytotoxin α-sarcin. (F) The 27-nucleotide duplex synthesized for NMR experiments. Numbering is based on the *X. laevis* 5S rRNA loop E. (G) A deletion mutant previously characterized in our laboratory (Varani et al., 1989). Numbering is based on the *X. laevis* 5S rRNA loop E. U_{73} was omitted to favor the base pairing proposed by Andersen et al. (1984).

† This research was supported in part by National Institutes of Health Grant GM 10840, by the U.S. Department of Energy, Office of Energy Research, Office of Health and Environmental Research, under Grant DE FG03-86ER60406, and through instrumentation grants from the U.S. Department of Energy (DE FG05-86ER75281) and from the National Science Foundation (DMB 86-09305 and BBS 87-20134).

‡ Present address: Department of Molecular Biology, MB2, the Scripps Research Institute, 10666 N. Torrey Pines Rd., La Jolla, Ca 92037.

§ Present address: MRC Laboratory of Molecular Biology, Hills Road, Cambridge, CB2 2QH, England.

0006-2960/93/0432-1078$04.00/0

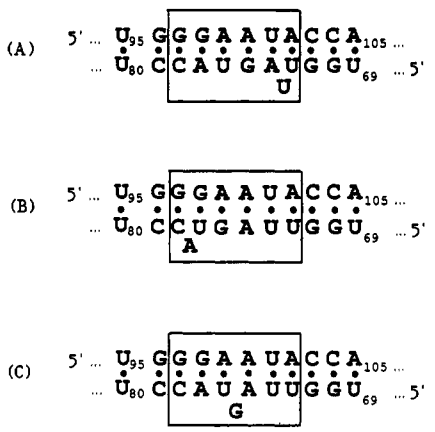

FIGURE 2: Models for the base pairing in *X. laevis* 5S rRNA loop E. The models in (A) and (B) are based on reactivity to chemical and enzymatic probes. The boxes enclose the loop and the loop-closing base pairs. (A) Model of Andersen et al. (1984). The bulged nucleotide, U_{73}, was proposed to be extrahelical. (B) Model of Romaniuk et al. (1988). The bulged nucleotide, A_{77}, was proposed to be intrahelical. (C) Results of the present NMR study. The bulged nucleotide, G_{75}, is extrahelical.

Westhof et al., 1989). However, different base-pairing schemes were proposed on the basis of these data (Figure 2A,B). Clearly, a higher-resolution biophysical technique is needed to define this structure. In this study, NMR spectroscopy followed by restrained molecular dynamics calculations was used to determine the conformation of a 27-nucleotide RNA (Figure 1F) containing the eukaryotic 5S rRNA loop E sequence. The NMR spectra and the structural model for the loop E are compared with those of a previously characterized single-nucleotide deletion mutant (Varani et al., 1989).

MATERIALS AND METHODS

RNA Synthesis and Purification. The two strands of the duplex, 5'-pppGGCGGAAUACCGC (strand 1) and 5'-pppGCGGUUAGUACGCC (strand 2), were synthesized separately using T7 RNA polymerase and the appropriate synthetic DNA templates (Milligan et al., 1987; Wyatt et al., 1991). Crude RNA was purified using denaturing polyacrylamide gel electrophoresis. Yields of RNA were 3–10 optical density units (ODU) of RNA per milliliter of reaction for strand 1, and 1–4 ODU/mL of reaction for strand 2. RNA samples were dialyzed extensively (>24 h) against a buffer with a high concentration of EDTA (150 mM NaCl, 10 mM sodium phosphate, and 5 mM Na_2EDTA, pH 6.4) to remove divalent cations and other impurities. The sequences were verified by enzymatic RNA sequencing reactions using RNases T_1, A, U_2, and CL3.

Selective Deuteration. GTP was deuterated at the 8 position to an extent of >90% by heating to 50 °C in 99.8% D_2O (Aldrich), pH 6, for 24 h. ATP was similarly deuterated to an extent of ca. 50% by heating to 50 °C at pH 6 for 48 h. In a separate reaction, ATP was deuterated at both the 2 (70% D) and 8 (ca. 100% D) positions by a catalytic exchange reaction. ATP (100 mg) and Pd/C catalyst (40 mg) were suspended in 1 mL of 99.8% D_2O and stirred under positive D_2 pressure at 22 °C for 24 h, and filtered. The progress of the deuteration reactions was monitored by NMR. All deuterated NTPs were used without repurification in T7 synthesis reactions since there did not appear to be a significant inhibition of polymerase activity by the NMP and/or NDP species resulting from NTP hydrolysis in the deuteration reaction.

UV-Induced Cross-Linking. RNA was 5'-labeled with [γ-^{32}P]ATP using T4 polynucleotide kinase (United States Biochemical) and purified on a denaturing 20% polyacrylamide gel. The product band was visualized by autoradiography, excised, eluted, and ethanol-precipitated with a 100-fold excess of the unlabeled complementary strand. Dried pellets were dissolved in 150 mM NaCl, 10 mM sodium phosphate, and 1 mM NaEDTA, pH 6.5, heated to 70 °C for 1 min, and then allowed to cool to 0 °C for 30 min prior to irradiation for 10–30 min with an ultraviolet lamp (designed for sterilization) while in contact with a large water/ice bath; 10 M urea/xylene cyanol loading buffer was then added, and the samples were heated to 90 °C for 1 min prior to being loaded on a denaturing 20% acrylamide gel for separation of cross-linked from non-cross-linked strands.

NMR Spectroscopy. NMR samples were dialyzed for at least 24 h against 150 mM NaCl, 10 mM sodium phosphate, and 0.01 mM EDTA, pH 6.5. Samples used for nonexchangeable proton experiments were lyophilized several times from D_2O before dissolution in 99.96% D_2O (Aldrich). Samples for exchangeable proton spectra were lyophilized, dissolved in 90% H_2O/10% D_2O, and adjusted to the desired pH (5.5 or 6.4). Sample concentrations were 1.5–2.5 mM in duplex. Experiments were done on GE GN-500, Bruker AMX-600, or Bruker AMX-400 instruments.

One-dimensional spectra in 90% H_2O/10% D_2O were collected using the 1331 sequence for solvent suppression (Hore, 1983). One-dimensional NOE spectra were obtained by irradiating for 400–600 ms with a low-power decoupler setting prior to the observation sequence. Irradiated and nonirradiated spectra were acquired in an interleaved manner to reduce the effect of instrumental instability.

For all two-dimensional experiments, pure-phase spectra were obtained using the TPPI method (Marion & Wüthrich, 1983) and attenuation of the residual HDO resonance by low-power presaturation during the relaxation delay. Typically, 2K complex points in t_2 and 400–450 points in t_1 were collected with spectral widths of 4000 or 4800 Hz for experiments collected at 500 or 600 MHz, respectively. The total relaxation delay was 2–2.5 s.

NOESY spectra in D_2O were acquired at 30 and 41 °C with a mixing time of 400 ms. J-peaks arising from zero-quantum coherences were shifted by incrementation of the mixing time with t_1 (Macura et al., 1982). Additional NOESY spectra were collected with mixing times of 60, 100, and 120 ms for quantitation of the NOE intensities. NOESY spectra in H_2O were collected at 600 MHz with a spectral width of 12 000 Hz and a mixing time of 150 ms. 4K complex points were collected in t_2, and 400 in t_1. Solvent suppression was obtained with the 1-1 sequence for the final "read" pulse.

A high-resolution, phosphorus-decoupled, double-quantum-filtered COSY specrum was collected at 600 MHz with a spectral width of 1500 Hz, 2K points in t_2, and 640 points in t_1. Phosphorus decoupling was achieved with a π ^{31}P pulse during t_1 and with GARP (Shaka et al., 1985) during t_2. A double-quantum spectrum was collected with an excitation delay of 50 ms and with a composite π pulse in the preparation period. An MLEV-17-based TOCSY spectrum was collected with a mixing time of 150 ms. A ^{1}H-detected heteronuclear-correlated ^{31}P–^{1}H spectrum was acquired at 400 MHz (^{1}H) with spectral widths of 1000 Hz (^{31}P) and 1500 Hz (^{1}H). 1K data points were acquired in t_2 and 140 in t_1, with a relaxation delay of 2.5 s and a total acquisition time of ca. 30 h. A natural-abundance ^{13}C–^{1}H HMQC spectrum was acquired at 600 MHz with sweep widths of 20 000 Hz (^{13}C) and 5000

Hz (^{1}H), with GARP decoupling during acquisition and the phase cycle proposed by Cavanagh and Keeler (1988). 1K data points were acquired in t_2 and 110 in t_1, with a relaxation delay of 2.5 s and a total acquisition time of 42 h.

Spectral Analysis. NMR data were processed on a μVAX using FTNMR (Hare Research, Inc.). Typically, spectra were zero-filled to 1K real points in t_1 prior to Fourier transformation, and a skewed, phase-shifted sine-bell (skew 0.7, phase shift 20–60°) was used in both dimensions for apodization.

Sugar puckers were determined from values of $J_{1'2'}$ taken from the H1′–H2′ cross-peaks in the high-resolution 2QF-COSY. Most H1′ resonances showed no cross-peak to H2′; an upper bound of 3 Hz was used for these couplings. Puckers were calculated from $J_{1'2'}$ according to equations given in Altona (1982), assuming a pucker amplitude of ≈35°. Proton–proton distance restraints were obtained from integration of NOE cross-peaks in short mixing time (60, 100, and 120 ms) NOESY experiments. NOEs were simply classified as strong, medium, and weak, with corresponding distance restraints of 1.8–3.0, 2.5–4.0, and 3.0–5.0 Å, respectively. Distance restraints corresponding to NOEs involving exchangeable protons were set to 1.8–5.0 Å, except for the particularly intense G_5 imino–U_{21} H5 NOE, which was set to 1.8–4.0 Å.

Structure Modeling. Restrained molecular dynamics (rMD) were calculated using the X-PLOR software package (Brünger, 1990). In order to speed the calculations, only two base pairs from each stem were included. The stems were modeled as canonical A-form helices using 98 interatomic distance restraints, 52 torsion angle restraints (20 backbone angle and 32 endocyclic sugar torsion angle restraints, ν_0–ν_3), and hydrogen-bonding restraints for the Watson–Crick base pairs. Error limits on these modeled A-form restraints were tight (±0.1 Å for distances and ±10° for all torsion angles except for ν_0–ν_3, which had an error of ±5°). A total of 125 experimental NOE and 36 experimental endocyclic sugar torsion angle (ν_0–ν_3) restraints were used to define the loop conformation. Structure modeling consisted of two stages. In the first stage, the global fold was calculated using a simulated annealing strategy. Twenty-three starting structures with randomized α, β, γ, ϵ, and ζ torsion angles were generated using the internal coordinate facility of version 2.1 of X-PLOR. Structures were calculated using a simulated annealing protocol slightly modified from that described in the X-PLOR manual (Brünger, 1990). Bond length and bond angle force constants were set to 1000 kcal mol^{-1} Å^2 and 500 kcal mol^{-1} rad^2, respectively. NOE and torsion angle force constants were 50 kcal mol^{-1} Å^2 and 50 kcal mol^{-1} rad^2, respectively. During the global fold calculation, all electrostatic interactions were turned off, and the repulsive-only van der Waals potential was used. In the second stage of refinement (modeling), converged global fold structures were again subject to rMD refinement, adding restraints for hydrogen bonds for mismatched base pairs (see Results). In this stage of refinement, electrostatic interactions and the Lennard–Jones van der Waals potential were turned on.

RESULTS

UV-Induced Cross-Linking

When irradiated with ultraviolet light, loop E in the intact HeLa 5S rRNA forms an interstrand covalent cross-link between G_{98} and U_{76} (Branch et al., 1985). Since the model loop E oligonucleotide contains the same loop sequence (Figure 1F), we tested the oligonucleotide for cross-link formation. The 27-mer oligonucleotide forms an interstrand cross-link

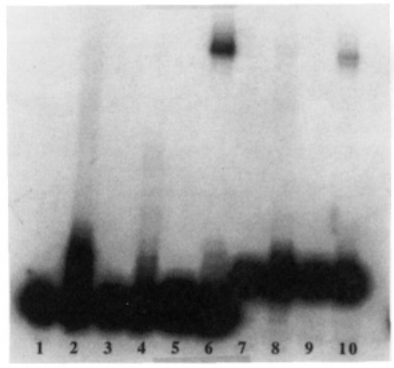

FIGURE 3: Ultraviolet-induced cross-linking of two oligonucleotide models for loop E (wild type, Figure 1F; single-nucleotide deletion mutant, Figure 1G). Denaturing PAGE was used to separate cross-linked from un-cross-linked molecules (see Materials and Methods for details). In lanes 1–6, strand 1 was labeled; in lanes 7–12, strand 2 was labeled. Lane 1, strand 1 control. Lane 2, irradiated strand 1 control. Lane 3, mutant control. Lane 4, irradiated mutant. Lane 5, wild-type control. Lane 6, irradiated wild type. Lane 7, strand 2 control. Lane 8, irradiated strand 2 control. Lane 9, wild-type control. Lane 10, irradiated wild type.

when irradiated with UV light (Figure 3, lanes 6 and 10). On the other hand, a single-nucleotide deletion mutant (Figure 1G) with identical stems fails to form the cross-link (Figure 3, lane 4), indicating that the cross-link occurs in the loop. No attempt was made to identify directly which nucleotides were cross-linked. The ability of the model oligonucleotide internal loop to undergo UV-induced interstrand cross-linking suggests that its conformation is very close to the native conformation of the internal loop E in intact 5S rRNA.

NMR Analysis

Exchangeable Proton Spectra. The imino portion of the proton NMR spectrum of the 27-mer oligonucleotide is plotted in Figure 4B. The more downfield-shifted imino resonances (11.9–13.6 ppm) arise from base-paired imino protons in the stems. The presence of several upfield-shifted resonances (10.0–11.6 ppm) from the loop suggests that the internal loop adopts a closed conformation, possibly including non-Watson–Crick base pairs. Indeed, four of a maximum possible of five loop imino protons are sufficiently protected from exchange with solvent to allow observation of their resonances. The two more downfield-shifted (11.22 and 11.57 ppm) loop imino resonances are sharper than the two more upfield-shifted ones. Their chemical shifts and the narrower line widths are consistent with participation of these iminos in hydrogen bonds. In contrast, the spectrum of the single-nucleotide deletion mutant (Varani et al., 1989; Figure 4A) contains no upfield imino resonances. Attempts to favor mismatch formation by lowering the temperature and raising the salt concentration did not result in the observation of new imino resonances (Varani et al., 1989). These data indicate that deletion of U_{73} results in the destabilization of the closed structure formed by this internal loop.

The imino spectrum was assigned by one- and two-dimensional NOE experiments. Of particular interest is the G_{98} imino resonance (11.57 ppm), which shows a sequential NOE to the imino resonance at 12.82 ppm (G_{97}), as well as unusual interstrand NOEs to both the H5 and H6 of U_{76} (5.95 and 8.05 ppm; Figure 4C) and to several sugar protons. The G_{98} imino–U_{76} H5 NOE is particularly intense, especially considering the relatively broad line width of this imino resonance. These are the residues which are cross-linked by exposure to ultraviolet light (Branch et al., 1985).

Despite the assignment of several of the loop imino proton resonances, it was not possible to establish geometries for loop

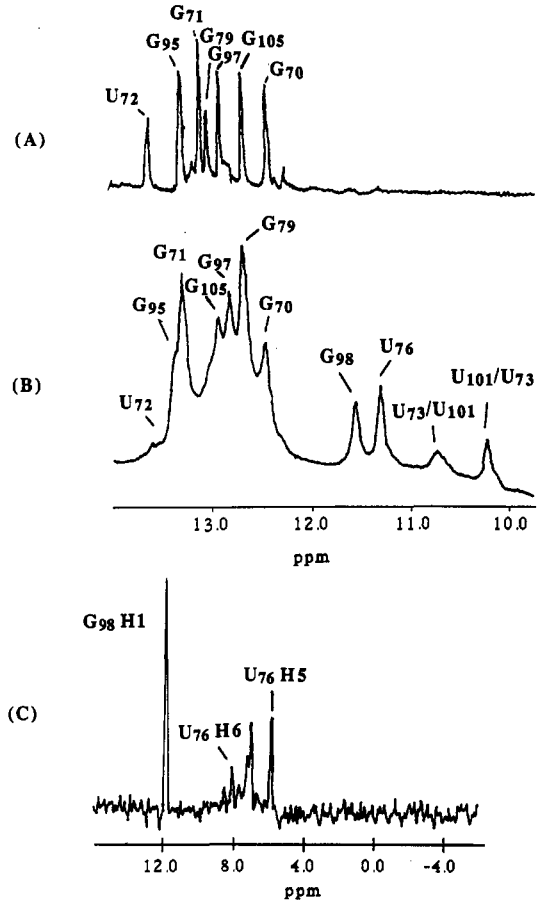

FIGURE 4: Comparison of the imino proton spectra of deletion mutant (A) and wild-type (B) loop E model oligonucleotides in 150 mM NaCl, 10 mM sodium phosphate, 0.01 mM EDTA, pH 6.4, 10 °C. Numbering is based on the sequence of the *X. laevis* oocyte 5S rRNA. The broader line width of the resonances of the wild-type oligonucleotide is due to nonspecific aggregation; at higher temperatures, the line widths of the two oligonucleotides are similar. (C) A slice through the 150-ms NOESY spectrum of the wild-type loop E model oligonucleotide in 90% H_2O/10% D_2O at 10 °C. The diagonal peak of the G_{98} H1 (imino) resonance at 11.57 ppm and unusual interstrand cross-peaks from it to the U_{76} H5 (5.95 ppm) and H6 (8.05 ppm) are labeled.

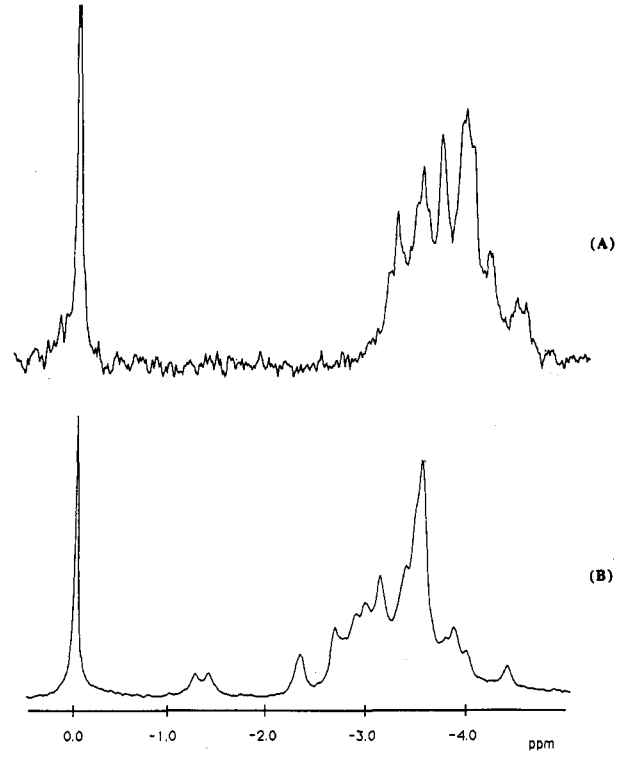

FIGURE 5: 162-MHz proton-decoupled ^{31}P spectra of model loop E oligonucleotides in 150 mM NaCl, 10 mM sodium phosphate, 0.01 mM EDTA, pH 6.4, 30 °C. Chemical shifts are relative to the phosphate buffer. (A) Single-nucleotide deletion mutant. (B) Wild type.

mismatches from NOEs involving exchangeable protons. The loop imino resonances are broad and, with the exception of the G_{98} imino proton, show few NOEs to other protons. In addition, the extensive overlap of the amino proton spectrum and the tendency of the sample to aggregate at low temperature and pH prevented assignment of most amino proton resonances.

^{31}P Spectrum. ^{31}P chemical shifts in nucleic acids are sensitive to the conformation about the torsion angles α and ζ and, to a lesser degree, β and ϵ (Gorenstein, 1984). Thus, the unusually well-dispersed ^{31}P spectrum of the 27-mer oligonucleotide (Figure 5B) suggests a varied and unusual backbone conformation. Two resonances are particularly downfield-shifted (ca. 1 ppm). Assignments of the ^{31}P spectrum from two-dimensional heteronuclear correlation confirmed that the unusually shifted resonances are from the loop region (data not shown). In contrast, the ^{31}P spectrum of the deletion mutant has the much narrower dispersion typical of helical nucleic acids (Varani et al., 1989; Figure 5A). This is again consistent with the hypothesis that deletion of U_{73} results in the opening of an unusual, closed structure formed by loop E in 5S rRNA.

Assignment of the Nonexchangeable Proton Resonances. The first step in the assignment process was the identification of the individual sugar spin systems (Varani & Tinoco, 1991). For the several residues with resolved H1′–H2′ couplings, correlated spectra (2QF-COSY, 2Q, TOCSY) were very useful in establishing sugar spin systems. For the two nucleotides (A_{74} and G_{75}) with $C_{2'}$-endo sugar pucker, identification of the H2′ and H3′ resonances was easily obtained from the 2QF-COSY spectrum. The small (<2 Hz) $J_{3'4'}$ of $C_{2'}$-endo sugars prevented extension of the connectivity to the H4′ resonances. For resonances with predominantly $C_{3'}$-endo pucker, the information from correlated spectra was much more limited, and assignments were mostly based on short mixing time NOESY experiments (60–120 ms). At very short mixing time (60 ms), the short and sugar pucker-independent H1′–H2′ distance (2.5–2.8 Å) produces the strongest NOEs to the H1′ protons. At longer mixing times (100–120 ms), the cross-peaks between the H1′ and H3′ and several H4′ resonances become observable either directly or by spin diffusion.

Once the individual sugar spin systems are identified, sequence-specific assignments can be obtained for small (<15–20 nucleotide) RNAs by a combination of ^1H–^{31}P COSY and ^1H–^1H correlated spectra, without the necessity of conformational assumptions (Varani & Tinoco, 1991). However, the severe overlap of the H3′, H4′, and H5′/H5″ resonances limited the number of assignments obtainable with this strategy, despite the favorable chemical shift dispersion of many loop resonances. Assignments were therefore based mostly on NOESY spectra. Although this approach may be subject to misassignments for unusual conformations, A-form connectivities were observed in the "fingerprint" region (aromatic to H1′) of NOESY spectra for both the stems and most of the loop of this oligonucleotide (Figure 6). This observation indicates the conservation of A-like stacking through most of the molecule, making NOESY-based sequence-specific assignments more reliable. The connectivities

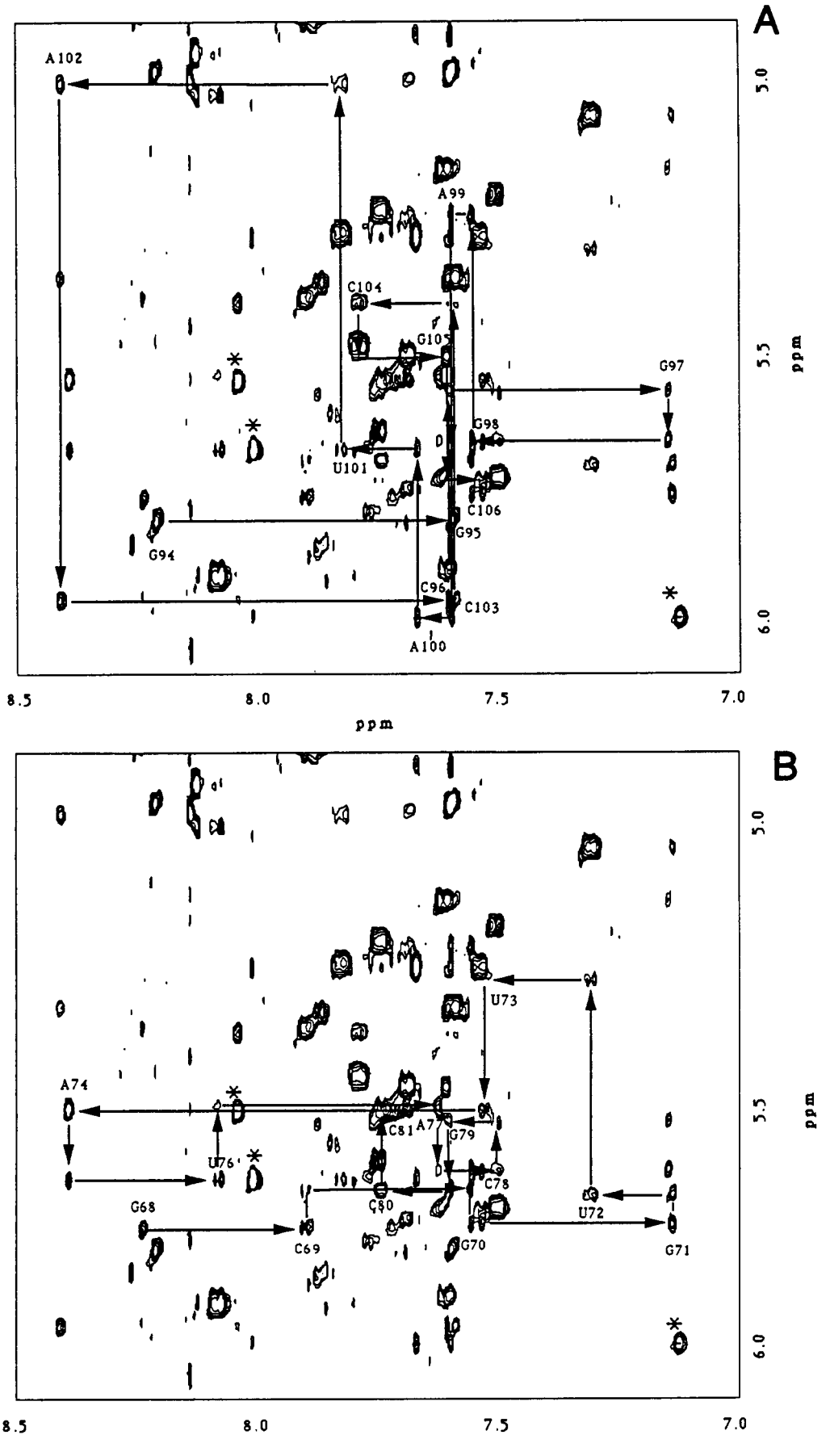

FIGURE 6: Aromatic proton to H1′ portion of the 400-ms NOESY spectrum of the wild-type loop E model oligonucleotide (Figure 1F) at 30 °C. Asterisks indicate intense NOEs between AH2 and H1′ protons. (A) NOE connectivities for strand 1; (B) NOE connectivities for strand 2. The A_{74} H1′ to U_{76} H6 NOE indicates that G_{75} is bulged out.

Table I: Chemical Shift Assignments (ppm) for the Wild-Type Loop E Oligonucleotide at 30 °C in 150 mM NaCl/0.01 mM EDTA, pH 6.4[a]

residue	H8/H6	H2/H5	H1′	H2′	H3′	H4′	H5′/H5″	imino	amino
G94	8.17	na	5.84	4.97	4.76	4.61	4.24/4.08		
G95	7.59	na	5.93	4.57	4.59	4.24		13.34	
C96	7.60	5.16	5.59	4.71	4.13	4.41		na	8.29, 6.67
G97	7.16	na	5.68	4.70	(4.61)			12.82	
G98	7.55	na	5.25	4.36	4.20			11.57	
A99	7.59	7.98	6.03	**5.29**	4.26	(4.89)		na	
A100	7.66	8.10	5.70	4.80	4.57	(4.23)		na	
U101	7.81	5.28	**4.99**	4.27	4.44			10.46 or 10.22	
A102	8.36	8.01	5.99	4.49	4.78		(4.28)	na	
C103	7.59	5.37	5.42	4.26	4.43	4.12		na	8.46, 7.13
C104	7.78	5.50	5.52	4.54	4.58	4.43	(4.11)	na	8.45, 6.82
G105	7.60	na	5.76	4.45				12.95	
C106	7.54	5.28	5.78	4.04	4.19	(4.32)		na	
G68	8.19	na	5.79	4.85	4.76	4.60	4.30/(3.92)	13.25	
C69	7.88	5.40	5.72	4.72	4.60			na	8.60, 6.82
G70	7.53	na	5.79	4.64	4.54			12.45	
G71	7.16	na	5.73	4.50	4.34	4.43	4.04	13.29	
U72	7.32	5.05	5.32	4.29	4.10	(4.38)	(4.00)/4.11	13.6	na
U73	7.53	**4.82**	5.57	4.19	4.46			10.46 or 10.22	
A74	8.34		5.70	**3.88**	4.75	4.98		na	
G75	8.09	na	5.94	4.93	**5.01**	4.39	(4.15/4.58)		
U76	8.05	5.95	5.56	4.74	(4.59)	(4.27)		11.29	
A77	7.62	7.14	5.68	4.82	(4.78)			na	
C78	7.50	5.75	5.59	(4.32)				na	8.45, 7.21
G79	7.59	na	5.72	4.54	4.59			12.69	
C80	7.73	5.23	5.56	4.26	(4.48)			na	8.51, 6.95
C81	7.68	5.51	5.78	4.03	4.20				

[a] Values in parentheses are tentative; values in boldface are unusual. na = not applicable.

expected for regular helical nucleic acids were also observed in other regions of the spectrum, and provided conclusive support for the initial assignments based on the H1′–aromatic connectivities of Figure 6. The assignments for the single-nucleotide mutant (Varani et al., 1989) served as a further control for the helical stems. In order to verify the loop assignments, and to resolve some ambiguities in the identification of adenine H2 resonances, assignments were confirmed by selective deuteration and by natural-abundance ^{1}H–^{13}C correlation. Strong attenuation or disappearance of NOESY cross-peaks for samples selectively deuterated at purine H8 and/or AH2 positions (Varani & Tinoco, 1991) allowed the confirmation of almost all loop H8 and AH2 assignments.

The spectral assignments are summarized in Table I. Many loop resonances (in boldface type) show uncommon chemical shifts, presumably as a result of an unusual loop conformation. There are considerable differences (up to 1 ppm) in chemical shifts between these assignments and those previously reported for the deletion mutant (Varani et al., 1989), confirming the large conformational differences between these very similar sequences. The chemical shifts are essentially identical (within 0.1 ppm) in the stems, with the exception of the loop-closing base pairs. Thus, the influence of changes in loop conformation does not extend beyond the loop-closing base pairs.

The conventional connectivity walks in the aromatic proton-to-H1′ region of the NOESY spectrum are observed for both stems (strand 1, Figure 6A; strand 2, Figure 6B). However, the conformations of the two strands differ remarkably. Essentially A-form connectivities are observed throughout strand 1, except for an unusually weak NOE between G_{97} H2′ and G_{98} H8, suggesting imperfect stacking at the stem–loop junction. The conformation of strand 2, on the other hand, shows some striking differences from A-form geometry. The NOE from A_{74} H1′ to U_{76} H6 (Figure 6B) demonstrates that G_{75} is bulged out. In addition, unusual sugar–sugar and base–sugar NOEs are seen between U_{73} and A_{74}. As with G_{97} and G_{98} on strand 1, only weak NOEs connect A_{77} and C_{78}, which again suggests poor stacking between the stem and the loop. Interstrand NOEs provide important structural information. In addition to the NOEs between the G_{98} imino proton and the base protons of U_{76} (Figure 4C), strong NOEs are observed from A_{77} H2 to the A_{99} H2 and the A_{99} H1′, and from A_{102} H2 to U_{73} H1′.

Sugar Puckers and Glycosidic Torsion Angles. The sugar conformation of each nucleotide was obtained from values of $J_{1'2'}$ from a high-resolution 2QF-COSY (see Materials and Methods). The absence of most H1′–H2′ cross-peaks in correlated spectra shows that most nucleotides adopt the predominantly N-type (close to $C_{3'}$-endo) pucker found in A-form helices. However, the bulged residue and the residue 5′ to it, A_{74} and G_{75}, are >90% $C_{2'}$-endo. An intermediate value for $J_{1'2'}$ was found for A_{102}, consistent with a 70%/30% mixture of S-type and N-type puckers. Spectral overlap prevented the measurement of other sugar coupling constants ($J_{2'3'}$, $J_{3'4'}$), or overall multiplet widths, needed to define the sugar conformation more accurately (Altona, 1982; Davis, 1989).

Glycosidic torsion angles were calculated from a comparison of experimental and theoretical intranucleotide sugar proton–aromatic proton distances (Wüthrich, 1986). When spectral overlap prevented more precise determination, the glycosidic torsion angle was classified simply as anti. There are no syn nucleotides, as had been proposed in previous models of the structure of loop E from base reactivity to chemical probes (Westhof et al., 1989). As demonstrated by selective deuteration and ^{1}H–^{13}C correlation experiments, all of the very intense purine base proton–H1′ NOESY cross-peaks (asterisked in Figure 6) originate from AH2 protons.

Structure Determination. Using random torsion angle starting structures, 23 preliminary structures were generated by rMD-simulated annealing as described under Materials and Methods. Of these structures, 12 have very similar restraint violation energies (<40 kcal/mol) and were judged to have converged; the other 11 have much higher energies and are probably trapped in local energy minima. Superposition of the converged structures revealed that the overall

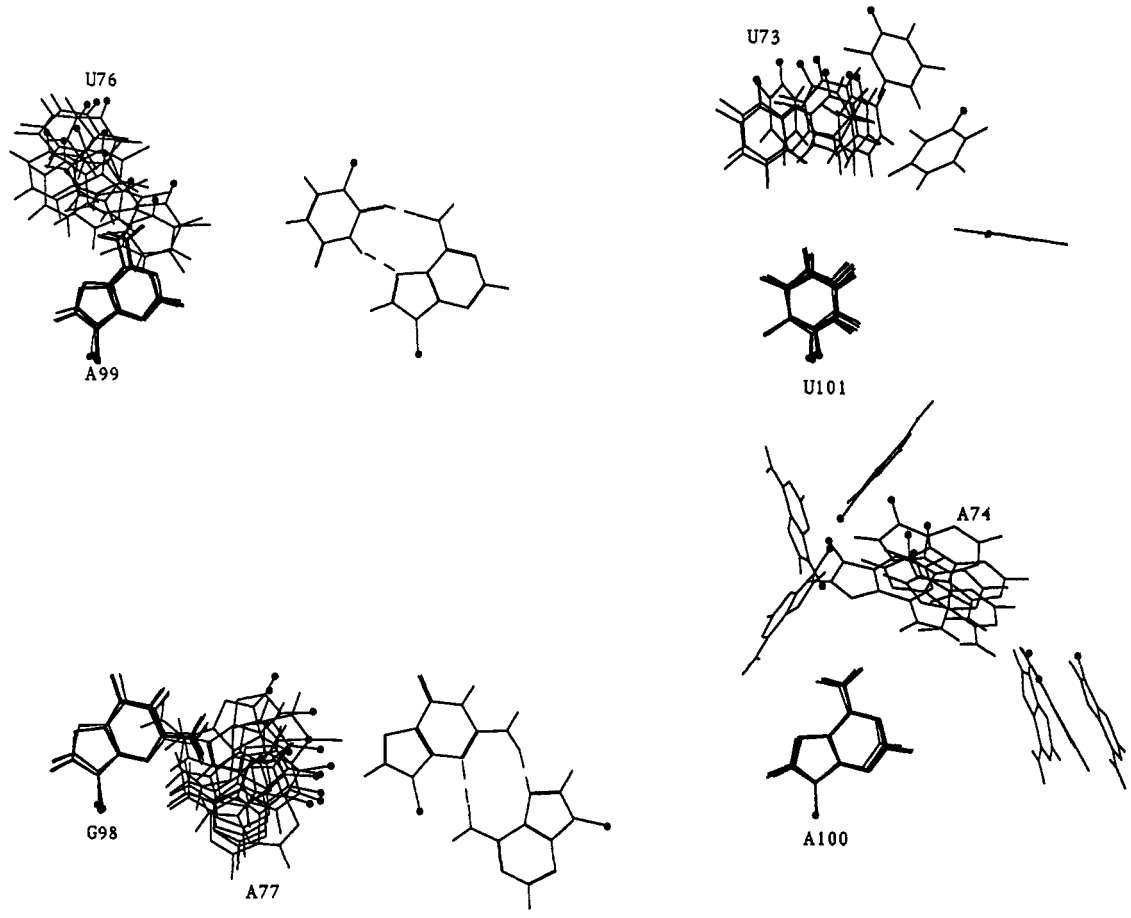

FIGURE 7: Relative orientation of loop bases in the wild-type loop E model oligonucleotide. Twelve converged rMD structures were superimposed using only a single nucleotide from strand 1 (G_{98} to U_{101}) for superposition. C1′ atoms are enlarged for clarity. The structures of the G_{98}·A_{77} and A_{99}·U_{76} appositions are much better determined than those of the A_{100}·A_{74} and U_{101}·U_{73} appositions. Proposed base pairs for G_{98}·A_{77} and A_{99}·U_{76} are also shown.

structure is not well determined (the average all-atom RMSD was 3.3 Å). However, a more detailed comparison of the structures revealed that many local features are well determined. The relative orientation of G_{98} and A_{77} (Figure 7) is close to that found in the G·A mismatches found in the GCAA hairpin loop (Heus & Pardi, 1991) and in a DNA duplex (Li et al, 1991). Similarly, A_{99} and U_{76} are close to the geometry expected for a reverse-Hoogsteen pair (Figure 7). While these superpositions do not rigorously prove the existence of interstrand hydrogen bonding, they do show that if hydrogen bonding occurs between G_{98} and A_{77} and between A_{99} and U_{76}, the resulting mispairs must have the geometries shown in Figure 7. The quality of these superpositions is in fact strong evidence for mismatched base pair formation since no direct hydrogen bond restraints for these mispairs were used. On the other hand, the relative orientations of A_{100} and A_{74} and of U_{101} and U_{73} vary widely among converged structures (Figure 7). Although the presence of cross-strand NOEs involving the adenine H2 resonances strongly suggests a closed conformation containing mismatched base pairs, the NMR data alone are not sufficient to define the detailed geometry of these putative mismatched base pairs (A_{100}·A_{74} and U_{101}·U_{73}).

Two additional local conformational features are well determined by the data. All converged structures show A_{74} "reversed", so that the local strand direction is parallel to the other strand (Figure 8). Unusual sugar–sugar and base–sugar NOEs between U_{73} and A_{74} require this reversal. G_{75} is bulged into the major groove in all the converged structures (Figure 8). Unusual internucleotide sugar–sugar NOEs, together with the reversal of A_{74}, require that this nucleotide lie in the major groove.

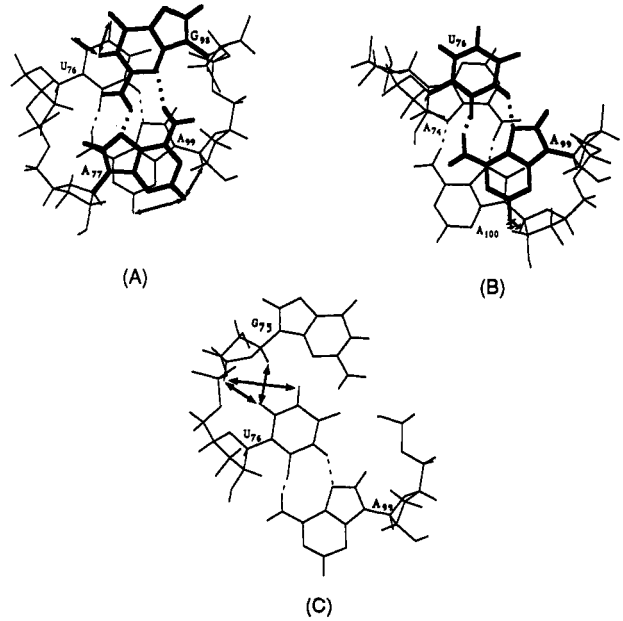

FIGURE 8: Views of base-pair stacking, with selected experimentally observed NOEs indicated by double-headed arrows. (A) Interstrand stacking of bases between the G_{98}·A_{77} and A_{99}·U_{76} pairs. (B) A possible symmetric A_{100}·A_{74} pair relative to the reverse-Hoogsteen A_{99}·U_{76} pair. A_{74} has an orientation parallel to the opposite strand. (C) The bulged nucleotide, G_{75}, may form a base-triple with the adjacent A_{99}·U_{76} pair.

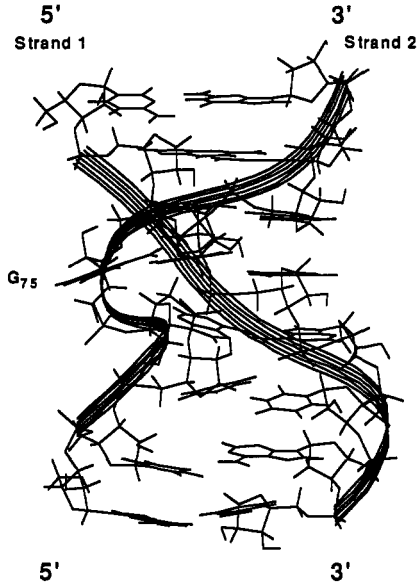

FIGURE 9: Ribbon diagram of the final model, emphasizing the irregularity of the backbone of strand 2 with the bulged G_{75}. Only two base pairs from each stem are shown.

At this point in the structure refinement, base-pairing constaints not directly reflected in the NMR data were added; we consider this final stage as modeling. Hydrogen-bond distance restraints for the G_{98}·A_{77}, reverse-Hoogsteen A_{99}·U_{76}, and a symmetric (N7-amino) A_{100}·A_{74} pair were added to the distance restraint file, and the electrostatic and attractive van der Waals interactions were turned on in the X-PLOR force field. The modeled symmetric A·A pair is consistent with both the NMR data and the chemical modification data of Romaniuk et al. (1988) (see Discussion). No assumption was made about the existence of the possible U_{101}·U_{73} pair, that was nonetheless found to form a pair with a geometry similar to that of a wobble G·U pair. This base pair might be present, perhaps mediated by a water molecule, as found in the crystal structure of a C·U base pair in a symmetric internal loop (Holbrook et al., 1991). In several refined structures, the G_{98} imino proton is within hydrogen-bonding distance of a phosphate oxygen from the opposite strand. The relative sharpness and chemical shift (11.57 ppm) of this imino resonance are consistent with hydrogen bonding, and the strong NOEs between this imino proton and several sugar proton resonances suggest a close contact with functional groups on the sugar–phosphate backbone on the opposite strand. Unfortunately, incomplete sugar spectral assignments (most H4′, H5′, and H5″ were not conclusively assigned) prevented the inclusion of these important constraints in the structure determination protocol. Conclusive identification of these possible base–backbone contacts would require experiments on ^{13}C-labeled oligonucleotides.

Figures 8 and 9 show several views of a typical refined model structure, including some very unusual experimentally observed NOEs. There is an unusually large winding angle (ca. 60°) between the G_{98}·A_{77} and the A_{99}·U_{76} pairs which increases interstrand stacking in the loop (Figure 8) and decreases stacking of the G_{98}·A_{77} base pair on the loop-closing G_{97}·C_{78} base pair. This poor stem–loop stacking is consistent with the observed weak NOE connectivities between these loop and stem nucleotides. The unusual interstrand stacking shown in Figure 8 may explain the observed ultraviolet-induced cross-link between G_{98} and U_{76}. Interestingly, the C1′–C1′ distance for all the loop mismatches is significantly less than in Watson–Crick base pairs (ca. 10.5 Å).

The structural role of the bulged residue, G_{75}, is not completely clear. While the position of its sugar moiety is fairly well determined, the base itself may occupy a fairly wide range of orientations. Nevertheless, the distance between the G_{75} amino nitrogen and the U_{76} O4 is less than 4 Å in all the refined structures; G_{75} may form a base-triple with the adjacent reverse-Hoogsteen pair by hydrogen-bonding one of its amino protons to the O4 of U_{76} (Figure 8). A ribbon diagram (Figure 9) contrasts the regular backbone of strand 1 with the irregular backbone of strand 2.

DISCUSSION

Precision of the Structure. NMR spectroscopy can provide high-resolution structures of RNA oligonucleotides with molecular masses of 3–5 kDa (Varani et al., 1991; Heus & Pardi, 1991; Varani & Tinoco, 1991). The quality of the structure depends on the number of torsion angle restraints used to define the conformation of the sugar–phosphate backbone (Wimberly, 1992). For isotopically unlabeled RNA oligonucleotides of higher molecular mass, spectral overlap of the sugar proton resonances severely limits the number of observable scalar couplings and, therefore, the number of available torsion angle restraints. A second problem with extended helical structures such as this internal loop is the small number of long-range distance restraints (other than the Watson–Crick hydrogen-bond restraints for the stem base pairs). In the case of the compact tetraloop structures (Varani et al., 1991; Heus & Pardi, 1991), unusual nonsequential NOEs between the loop nucleotides help define the structure. For this internal loop, the absence of hydrogen-bonding restraints for the non-Watson–Crick base pairs and the paucity of long-range NOEs limit the structural definition attainable. Although several cross-strand NOEs clearly demonstrate that the loop conformation is closed by base–base and, probably, base–backbone contracts, the precise geometry of the base pairs is difficult to define. For both reasons, the loop E structure presented here should not be seen as a final structure determination, but rather as a very significant step toward a high-resolution NMR structure that will require experiments on ^{13}C- and ^{15}N-labeled oligonucleotides. Three-dimensional NMR experiments on ^{13}C- and ^{15}N-labeled RNA would allow the determination of more NOE and backbone torsion angle restraints and should prove or disprove the structural features (e.g., the A·A base pair) which are only modeled at present.

Structural Features of Loop E. Although the present NMR restraint set determines the entire loop E structure only to low resolution, many local conformational features are well determined by unusual interstrand and sugar–sugar NOEs. Overall, the more highly conserved portion of the loop (Figure 1) is much better determined than the less-conserved A·A and U·U appositions. In particular, the unusual G_{98}·A_{77} and A_{99}·U_{76} base pairs (Figure 7) are fairly well-defined by intra- and interstrand NOEs involving nonexchangeable and imino protons (Figure 8), even without the use of direct hydrogen bond restraints. The poor definition of the less-conserved portion of the loop is consistent both with conformational dynamics and with a single conformation underdetermined by the available data. The lack of evidence for significant conformational dynamics suggests that this part of the structure is most likely underdetermined.

Interstrand stacking of the highly conserved G_{98}·A_{77} and reverse-Hoogsteen A_{99}·U_{76} base pairs rationalizes the experimental observation of the UV-induced cross-link between G_{98} and U_{76}. The strong NOEs between the G_{98} imino and the aromatic protons of U_{76} are clearly a result of the unusual

stacking of these bases (Figure 8). Extensive interstrand stacking associated with this geometry of the G·A pair has also been proposed for a DNA oligonucleotide (Li et al., 1991).

Perhaps surprisingly, G_{75} is bulged into the major groove and may be hydrogen-bonded to a neighboring reverse-Hoogsteen base pair. This putative base-triple would explain why a bulged nucleotide should be highly conserved (Figure 1), though G_{75} could also be important for protein recognition. Overall, strand 1 has a regular, almost A-form geometry, while strand 2 has a very irregular conformation to accommodate the extrusion of G_{75} and the reversal of A_{74} (Figures 8 and 9). Both of these nucleotides have $C_{2'}$-endo sugar pucker, consistent with previous observations that RNA nucleotides at turns are often $C_{2'}$-endo (Varani et al., 1991; Puglisi et al., 1990). The conformation of A_{74} is reversed, with the backbone pointing locally in the direction opposite to the rest of the helix (Figure 9). There is no obvious structural reason for this reversal other than the possible symmetric A_{74}·A_{100} base pair. If present, this base pair can explain the chemical modification data (see the next section), without any requirement for syn nucleotides. It must be emphasized, however, that the NMR data alone do not define this base pair unambiguously (Figure 7).

Comparison with Chemical and Enzymatic Probing. The structure of loop E has been modeled on the basis of chemical and enzymatic probing experiments (Andersen et al., 1984; Romby et al., 1988; Westhof et al., 1989). More recently, a rhodium probe has been used to map *X. laevis* 5S RNA (Chow et al., 1992). On the basis of the cleavage of tRNAs of known structure, the rhodium probe has been shown to cleave RNA preferentially at stem–loop junctions and at regions of tertiary structure, where a wider major groove is thought to allow intercalation of the probe. Mutagenesis of loop E residues suggested the presence of significant interaction between the two strands (either base-pairing or stacking) since mutations on one strand led to changes in reactivity on the opposite strand (Chow et al., 1992).

Two different models were proposed for loop E (Figure 2), but neither is fully consistent with the NMR data (Figure 6B). G_{75}, not U_{73}, is bulged out of the helix, and no nucleotides adopt the syn conformation about the glycosidic angle. However, the NMR model is in good agreement with the results of chemical and enzymatic mapping. G_{75} is the only purine base whose N7 atom is highly accessible to modification by DMS (Romaniuk et al., 1988; Westhof et al., 1989). The NMR data (Figure 6B) unambiguously show that G_{75} is bulged out; in all converged structures, G_{75} lies in the major groove with the N7 atom accessible to the solvent. Base pairing with G_{98} protects the A_{77} N7 atom from chemical modification. The proposed symmetric A_{100}·A_{74} base pair explains the observed N7 and N1 reactivities of these residues (both N7s unreactive, both N1s reactive) without requiring any syn nucleotides. It is not immediately clear from the NMR-derived structure, however, why the G_{98} N7 is protected. Experimentally, all the adenine N1 positions are reactive, and the G_{75} and G_{98} N1 atoms are protected. In all converged structures, the G_{98} N1 is inside the helix and inaccessible; in addition, several strong NOEs between the G_{98} imino proton and sugar protons suggest a possible interaction between this imino proton and the sugar–phosphate backbone of the opposite strand (Figure 8). The G_{75} N1 atom is less accessible than its reactive N7 (Figure 8), though the position of the base moiety of G_{75} must be regarded as underdetermined by the data (cf. Results). The reverse-Hoogsteen A_{99}·U_{76} and G_{98}·A_{77} base pairs leave both adenine N1 atoms relatively exposed (Figure 8). Finally, the possible U_{101}·U_{73} base pair is consistent with the protection of the uracil imino positions.

The observation of a UV-induced interstrand cross-link both in the 27-mer RNA and in the intact 5S rRNA suggests that the conformation of this oligonucleotide is very similar to that of loop E. Furthermore, the good correlation between the chemical reactivity in the intact 5S rRNA loop E and the surface accessibility of the NMR structure suggests that the NMR structure is a good model for loop E. The differences between the present NMR results and previous models probably lie in the interpretation of the chemical mapping experiments. While the chemical and enzymatic mapping experiments did suggest a closed conformation with unusual base pairs, more detailed features (the presence of syn nucleotides, which nucleotide is bulged, the base-pair geometry) were not correctly identified. More comparisons between solution structures determined by NMR and by chemical mapping will improve the power of low-resolution methodologies by identifying the actual structural targets of these probes.

Implications for Protein Recognition. The best-determined portion of the loop E structure roughly corresponds to its most highly conserved nucleotides. It is intriguing that very similar internal loops are found at both ends of the 23S-like rRNA and in the central conserved region of viroid RNAs (Figure 1). The repeated use of this structural element suggests an important functional role for these loop E-like internal loops. The loop pictured in Figure 1E, which is cleaved between G4325 and A4326 by the cytotoxin α-sarcin, appears to have an important role in translation (Nierhaus et al., 1992; Endo et al., 1991). Comparison of NMR spectra reported here and by Szewczak et al. (1991) strongly suggests that the conformation of this "alpha sarcin loop" is as depicted in Figure 1E: an extrastable tetraloop hairpin is separated from a loop E-like internal loop by a single Watson–Crick base pair. Such a tenuous separation suggests that the stability of the internal loop may strongly depend on the integrity of the hairpin structure. It is possible that the vital functions disrupted by α-sarcin cleavage are performed by the internal loop and that the function of the hairpin tetraloop is simply to stabilize the internal loop.

Alternatively, this internal loop motif may simply be a signal for protein recognition. The eukaryotic 5S rRNA loop E is part of the binding site for at least two proteins, the transcription factor IIIA (TFIIIA) (Romaniuk et al., 1987) and ribosomal protein L5 (Allison et al., 1991). Although TFIIIA binding decreases only slightly if loop E is extensively mutated to a Watson–Crick duplex (Romaniuk, 1989), loop E appears to make important contacts with TFIIIA (Darsillo & Huber, 1991). The unusual structure of this internal loop provides a number of easily recognizable potential binding signals: the bulged G_{75} in the major groove; the convoluted backbone of strand 2; and the narrow C1′–C1′ distances (a measure of groove width). Single-base bulges, such as G_{75} in our loop E model, may be a common feature of closed asymmetric internal loops; they are already known to be important for protein binding in several systems (Wu & Uhlenbeck, 1987; Gott et al., 1991).

The large difference in conformation between the wild-type loop E and a single-nucleotide deletion mutant implies that the effects of RNA mutations on protein–RNA recognition should be interpreted with caution. The model of Andersen et al. (1984) suggested that an oligonucleotide containing a mutant loop E without U_{73} would be a good model for the intact loop E. However, the conformation of

the mutant loop was found to be open, although transient base pair formation was not ruled out by the data (Varani et al., 1989). In contrast, the wild-type loop E sequence has a closed conformation containing several non-Watson–Crick base pairs. The conformation several residues away from the deletion is dramatically affected by what appeared to be a fairly neutral mutation. This surprising result emphasizes how little is presently known about the rules for base pairing and bulge formation in RNA internal loops. The stability of an interaction (mispair, base–phosphate hydrogen bonds, etc.) may be very sensitive to non-nearest-neighbor effects. More biophysical studies are needed to improve our understanding of the structure and stability of RNA internal loops. In the absence of structural information on an RNA internal loop, the effect of loop mutations on binding to a protein should not be interpreted solely in terms of a loss of intermolecular RNA–protein contacts. As this study shows, the RNA structure itself may be very significantly affected by the mutations in ways that cannot yet be reliably predicted.

ACKNOWLEDGMENT

It is a pleasure to acknowledge the laboratory manager, Ms. Barbara Dengler. We thank Mr. David Koh for synthesis of the DNA templates used in RNA synthesis and other members of the group for useful comments and discussions.

REFERENCES

Allison, L. A., Romaniuk, P. J., & Bakken, A. H. (1991) *Dev. Biol. 144*, 129–144.
Altona, C. (1982) *Recl. Trav. Chim. Pays-Bas 101*, 413–433.
Andersen, J., Delihas, N., Hanas, J. S., & Wu, C.-W. (1984) *Biochemistry 23*, 5752–5759.
Branch, A. D., Benenfeld, B. J., & Robertson, H. D. (1985) *Proc. Natl. Acad. Sci. U.S.A. 82*, 6590–6594.
Brünger, A. T. (1990) *X-PLOR: A System for Crystallography and NMR*, Yale University Press, New Haven, CT.
Cavanagh, J., & Keeler, J. (1988) *J. Magn. Reson. 77*, 356–362.
Cech, T. R. (1990) *Annu. Rev. Biochem. 59*, 543–568.
Chastain, M., & Tinoco, I., Jr. (1991) *Prog. Nucleic Acid Res. Mol. Biol. 41*, 131–177.
Chow, C. S., Hartmann, K. M., Rawlings, S. L., Huber, P. W., & Barton, J. K. (1992) *Biochemistry 31*, 3534–3542.
Darsillo, P., & Huber, P. W. (1991) *J. Biol. Chem. 266*, 21075–21082.
Davis, P. W. (1989) Thesis, University of California at Berkeley.
Ellington, A. D., & Szostak, J. W. (1990) *Nature 346*, 818–822.
Endo, Y., Gluck, A., & Wool, I. G. (1991) *J. Mol. Biol. 221*, 193–207.
Gorenstein, D. G. (1984) *Phosphorus-31 NMR: Principles and Applications* (Gorenstein, D. G., Ed.) Academic Press, New York.
Gott, J. M., Wilhelm, L. J., & Uhlenbeck, O. C. (1991) *Nucleic Acids Res. 19*, 6499–6503.
Gregory, R. J., Cahill, P. B., Thurlow, D. L., & Zimmermann, R. A. (1988) *J. Mol. Biol. 204*, 295–307.
Gutell, R. R., & Fox, G. E. (1988) *Nucleic Acids Res. 16, Suppl.*, r175–r269.
Heaphy, S., Finch, J. T., Gait, M. J., Karn, J., & Singh, M. (1991) *Proc. Natl. Acad. Sci. U.S.A. 88*, 7366–7370.
Heus, H. A., & Pardi, A. (1991) *Science 253*, 191–194.
Holbrook, S. R., Cheong, C., Tinoco, I., Jr., & Kim, S.-H. (1991) *Nature (London) 353*, 579–581.
Hore, P. J. (1983) *J. Magn. Reson. 55*, 283–300.
Keese, P., & Symons, R. H. (1985) *Proc. Natl. Acad. Sci. U.S.A. 82*, 4582–4586.
Li, Y., Zon, G., & Wilson, W. D. (1991) *Proc. Natl. Acad. Sci. U.S.A. 88*, 26–30.
Macura, S., Wüthrich, K., & Ernst, R. R. (1982) *J. Magn. Reson. 46*, 269–282.
Marion, D., & Wüthrich, K. (1983) *Biochem. Biophys. Res. Commun. 113*, 967–974.
Milligan, J. F., Groebe, D. R., Witherell, G. W., & Uhlenbeck, O. C. (1987) *Nucleic Acids Res. 15*, 8783–8798.
Nierhaus, K. H., Schilling-Bartetzko, S., & Twardowski, T. (1992) *Biochimie 74*, 403–410.
Noller, H. F., Hoffarth, V., & Zimniak, L. (1992) *Science 256*, 1416–1419.
Puglisi, J. D., Wyatt, J. R., & Tinoco, I., Jr. (1990) *Biochemistry 29*, 4215–4226.
Puglisi, J. D., Tan, R. Y., Calnan, B. J., Frankel, A. D., & Williamson, J. (1992) *Science 257*, 76–80.
Romaniuk, P. J. (1989) *Biochemistry 28*, 1388–1395.
Romaniuk, P. J., de Stevenson, I. L., & Wong, H. H.-A. (1987) *Nucleic Acids Res. 15*, 2737–2755.
Romaniuk, P. J., de Stevenson, I. L., Ehresmann, C., Romby, P., & Ehresmann, B. (1988) *Nucleic Acids Res. 16*, 2295–2312.
Romby, P., Westhof, E., Toukifimpa, R., Mache, R., Ebel, J.-P., Ehresmann, C., & Ehresmann, B. (1988) *Biochemistry 27*, 4721–4730.
Saenger, W. (1984) *Principles of Nucleic Acid Structure*, Springer-Verlag, New York.
Shaka, A. J., Barker, P. B., & Freeman, R. (1985) *J. Magn. Reson. 64*, 547–552.
Stern, S., Powers, T., Changchien, L. M., & Noller, H. F. (1989) *Science 244*, 783–790.
Szewczak, A. A., Chan, Y. L., Moore, P. B., & Wool, I. G. (1991) *Biochimie 73*, 871–877.
Varani, G., & Tinoco, I., Jr. (1991) *Q. Rev. Biophys. 24*, 479–532.
Varani, G., Wimberly, B., & Tinoco, I., Jr. (1989) *Biochemistry 28*, 7760–7772.
Westhof, E., Romby, P., Romaniuk, P. J., Ebel, J. P., Ehresmann, C., & Ehresmann, B. (1989) *J. Mol. Biol. 207*, 417–431.
Wimberly, B. (1992) Thesis, University of California, Berkeley.
Wolters, J., & Erdmann, V. A. (1988) *Nucleic Acids Res. 16, Suppl.*, r1–r70.
Wu, H.-N., & Uhlenbeck, O. C. (1987) *Biochemistry 26*, 8221–8227.
Wüthrich, K. (1986) *NMR of Proteins and Nucleic Acids*, John Wiley & Sons, New York.
Wyatt, J. R., Chastain, M., & Puglisi, J. D. (1991) *BioTechniques 11*, 764–769.